7. Santer, B. D. *et al.* Interpreting differential temperature trends at the surface and in the lower troposphere. *Science* **287,** 1227–1232 (2000).
8. Hansen, J. *et al.* Climate forcings in Goddard Institute for Space Studies SI2000 simulations. *J. Geophys. Res.* **107,** doi:10.1029/2001JD001143 (2002).
9. Ramaswamy, V. *et al.* Stratospheric temperature trends: Observations and model simulations. *Rev. Geophys.* **39,** 71–122 (2001).
10. Spencer, R. W. & Christy, J. R. Precise monitoring of global temperature trends from satellites. *Science* **247,** 1558–1662 (1990).
11. Hansen, J. *et al.* Satellite and surface temperature data at odds? *Clim. Change* **30,** 103–117 (1995).
12. Wallace, J. M. *et al. Reconciling Observations of Global Temperature Change* (National Academy Press, Washington DC, 2000).
13. Singer, S. F. Difficulty in reconciling global warming data. *Nature* **409,** 281 (2001).
14. Hegerl, G. C. & Wallace, J. M. Influence of patterns of climate variability on the difference between satellite and surface temperature trends. *J. Clim.* **15,** 2412–2428 (2002).
15. Santer, B. D. *et al.* Influence of satellite data uncertainties on the detection of externally forced climate change. *Science* **300,** 1280–1284 (2003).
16. Gaffen, D. J., Sargent, M. A., Habermann, R. E. & Lanzante, J. R. Sensitivity of tropospheric and stratospheric temperature trends to radiosonde data quality. *J. Clim.* **13,** 1776–1796 (2000).
17. Lanzante, J. R., Klein, S. A. & Seidel, D. J. Temporal homogenization of monthly radiosonde temperature data. *J. Clim.* **16,** 224–262 (2003).
18. Christy, J. R., Spencer, R. W. & McNider, R. T. Reducing noise in the MSU daily lower-tropospheric global temperature dataset. *J. Clim.* **8,** 888–896 (1995).
19. Christy, J. R., Spencer, R. W. & Lobl, E. S. Analysis of the merging procedure for the MSU daily temperature time series. *J. Clim.* **11,** 2016–2041 (1998).
20. Wentz, F. J. & Schabel, M. Effects of orbital decay on satellite-derived lower-tropospheric temperature trends. *Nature* **394,** 661–664 (1998).
21. Christy, J. R., Spencer, R. W. & Braswell, W. D. MSU tropospheric temperature: Dataset construction and radiosonde comparisons. *J. Atmos. Ocean. Technol.* **17,** 1153–1170 (2000).
22. Prabhakara, C., Iacovazzi, J. R., Yoo, J. M. & Dalu, G. Global warming: Evidence from satellite observations. *Geophys. Res. Lett.* **27,** 3517–3520 (2000).
23. Mo, T., Goldberg, M. D. & Crosby, D. S. Recalibration of the NOAA microwave sounding unit. *J. Geophys. Res.* **106,** 10145–10150 (2001).
24. Vinnikov, K. Y. & Grody, N. C. Global warming trend of mean tropospheric temperature observed by satellites. *Science* **302,** 269–272 (2003).
25. Spencer, R. W. & Christy, J. R. Precision and radiosonde validation of satellite gridpoint temperature anomalies. Part II: A tropospheric retrieval and trends during 1979–1990. *J. Clim.* **5,** 858–866 (1992).
26. Hurrell, J. W. & Trenberth, K. E. Spurious trends in satellite MSU temperature from merging different satellite records. *Nature* **386,** 164–167 (1997).
27. Trenberth, K. E. & Hurrell, J. W. Reply to "How accurate are satellite 'thermometers'?". *Nature* **389,** 342–343 (1997).
28. Hurrell, J. W. & Trenberth, K. E. Difficulties in obtaining reliable temperature trends: Reconciling the surface and satellite Microwave Sounding Unit records. *J. Clim.* **11,** 945–967 (1998).
29. Stone, P. H. & Carlson, J. H. Thermal equilibrium of the atmosphere with a given distribution of relative humidity. *J. Atmos. Sci.* **36,** 415–423 (1979).
30. Wentz, F. J. & Schabel, M. Precise climate monitoring using complementary satellite data sets. *Nature* **403,** 414–416 (2000).

Supplementary Information accompanies the paper on **www.nature.com/nature**.

Acknowledgements We thank J. M. Wallace for discussions. We also thank J. M. Wallace, D. L. Hartmann, J. R. Holton, J. K. Angell and M. Free for their comments on the manuscript. This study was supported by the US DOE, NSF and NASA.

Competing interests statement The authors declare that they have no competing financial interests.

Correspondence and requests for materials should be addressed to Q.F. (qfu@atmos.washington.edu).

Partitioning of oxygen during core formation on the Earth and Mars

David C. Rubie, Christine K. Gessmann* & Daniel J. Frost

Bayerisches Geoinstitut, University of Bayreuth, D-95444 Bayreuth, Germany

* Present address: Gleiwitzerstrasse 3, D-55131 Mainz, Germany

Core formation on the Earth and Mars involved the physical separation of metal and silicate, most probably in deep magma oceans[1–4]. Although core-formation models explain many aspects of mantle geochemistry, they have not accounted for the large differences observed between the compositions of the mantles of the Earth (~8 wt% FeO) and Mars (~18 wt% FeO) or the smaller mass fraction of the martian core[5–7]. Here we explain these differences as a consequence of the solubility of oxygen in liquid iron-alloy increasing with increasing temperature. We assume that the Earth and Mars both accreted from oxidized chondritic material. In a terrestrial magma ocean, 1,200–2,000 km deep, high temperatures resulted in the extraction of FeO from the silicate magma ocean owing to high solubility of oxygen in the metal. Lower temperatures of a martian magma ocean resulted in little or no extraction of FeO from the mantle, which thus remains FeO-rich. The FeO extracted from the Earth's magma ocean may have contributed to chemical heterogeneities in the lowermost mantle[8], a FeO-rich D″ layer[9] and the light element budget of the core[10,11].

The most significant differentiation event in the history of the Earth and other terrestrial planets was the separation of metal and silicate to form a metallic Fe-rich core and a silicate mantle. The geochemical consequences of this process have been studied extensively in recent years to explain the geochemistry of the Earth's mantle and the physical mechanisms of core formation and accretion. Extensive melting of the Earth and the formation of a deep magma ocean as a consequence of one or more giant impacts probably facilitated metal–silicate separation[12,13]. The content of moderately siderophile (metal-loving) elements, such as Ni and Co, in the Earth's mantle can be explained by the separation of liquid metal and silicate in a magma ocean at least 700 km deep[1–3]. This conclusion is based on experimental studies of the partitioning of siderophile elements between liquid metal and liquid silicate at high pressure. Here we consider the partitioning of oxygen between metal and silicate in a magma ocean with the aim of understanding how the FeO content and oxidation state of planetary mantles are affected by core formation.

We studied the solubility of oxygen in liquid Fe-Ni alloy at 9 and 18 GPa, 2,173–2,673 K and oxygen fugacities (f_{O_2}) 1.1 to 3.6 log units below the iron-wüstite buffer by equilibrating the samples with magnesiowüstite in a multianvil apparatus. Details of the starting materials and experimental and analytical methods have been described previously[14]. Over the range of experimental conditions, the solubility varies from below detection limit to 1.28 wt% (Fig. 1a, Table 1). The results show that oxygen solubility increases with increasing temperature and oxygen fugacity (Fig. 1a). To determine the effects of pressure and temperature independently of f_{O_2}, we calculate the distribution coefficient, K_d, for the partitioning of oxygen between liquid Fe-alloy and magnesiowüstite:

$$K_d = \frac{X_O^{met} X_{Fe}^{met}}{X_{FeO}^{mw}} \quad (1)$$

where X_O^{met}, X_{Fe}^{met} and X_{FeO}^{mw} are the mole fractions of oxygen in metal, Fe in metal and FeO in magnesiowüstite respectively. As shown in Fig. 1b, the distribution coefficient, and therefore the oxygen solubility at constant f_{O_2}, decreases with increasing pressure. These trends are consistent with previous results obtained at 5–25 GPa and 2,073–2,773 K but over a relatively restricted f_{O_2} range[15]. Note that the results are contrary to early predictions that the solubility of oxygen in liquid Fe should increase with increasing pressure[16].

To extrapolate the oxygen solubility data as a function of pressure (P) and temperature (T), we use:

$$RT\ln K_d = -\Delta H + T\Delta S - P\Delta V \quad (2)$$

where ΔH, ΔS and ΔV are the changes in enthalpy, entropy and volume, respectively, for the oxygen exchange reaction and R is the gas constant. We fitted equation (2) to the data, including five experimental results obtained up to 25 GPa by ref. 15. Results of the fit, shown in Fig. 1a and b, give $\Delta H = 153{,}000\ (\pm 29{,}000)$ J mol^{-1}, $\Delta S = 50.9\ (\pm 12.4)$ J K^{-1} mol^{-1} and $\Delta V = 1{,}448\ (\pm 440)$ J GPa^{-1} (1.448 ± 0.44 cm^3 mol^{-1}).

Extrapolations of the solubility results to higher pressures and

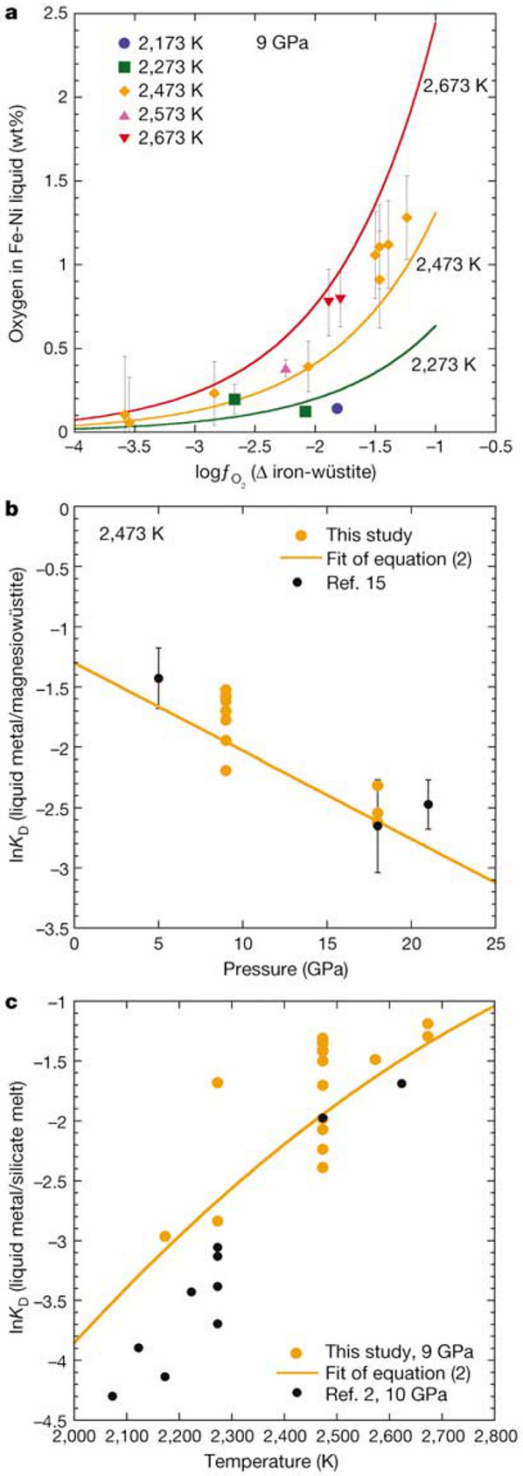

Figure 1 Oxygen partitioning results. **a**, **b**, Experimental results plotted as oxygen content in liquid Fe-alloy as a function of oxygen fugacity (f_{O_2}), relative to the iron-wüstite buffer, at 9 GPa and 2,173–2,673 K (**a**) and lnK_d as a function of pressure at 2,473 K; see equation (1) (**b**). At constant f_{O_2}, oxygen solubility increases with increasing temperature and decreases with increasing pressure. **c**, lnK_d for the partitioning of oxygen between liquid metal alloy and silicate melt calculated from liquid metal alloy/magnesiowüstite partitioning data, using equation (3). Values of lnK_d for oxygen partitioning between liquid Fe-Ni-S alloy and silicate melt, calculated from the results of ref. 2, are shown for comparison. The line is the fit of equation (2) to our data, modified using equation (3).

temperatures, using equation (2), are shown in Fig. 2. At moderate pressures (5–10 GPa) oxygen solubility is predicted to reach 5–15 wt% at 3,500–4,000 K. However, as pressure exceeds ~40 GPa, oxygen solubility becomes low, even at very high temperatures.

We examine the consequences of the partitioning of oxygen between liquid Fe-Ni metal and silicate liquid in a magma ocean. To determine the partitioning of oxygen between liquid metal and peridotite liquid in a magma ocean, we use the empirical relationship:

$$X_{FeO}^{mw} = 1.148X_{FeO}^{Sil} + 1.319\left(X_{FeO}^{Sil}\right)^2 \quad (3)$$

where X_{FeO}^{Sil} is the mole fraction of FeO in silicate liquid. Equation (3) has been derived using the results of melting studies of peridotite and Fe-rich peridotite bulk compositions[17,18]. Figure 1c shows the distribution coefficient K_d for the partitioning of oxygen between liquid Fe-alloy and silicate melt calculated from our liquid Fe-alloy/magnesiowüstite partitioning data using equation (3). These data and the recalculated fit of equation (2) are compared with previously published results on the partitioning of oxygen between liquid Fe-Ni-S alloy and silicate melt[2,19]. The similar temperature dependence and absolute values of K_d observed indicates that the addition of up to 30 wt% sulphur has a very minor effect on oxygen solubility (Fig. 1c).

For a given bulk composition, the equilibrium compositions and mass fractions of coexisting metal and silicate are calculated by mass balance using equations (2) and (3). We consider the geochemical consequences of metal–silicate separation using a polybaric metal–silicate fractionation model[20]. We assume that the temperature at the base of the magma ocean is defined by the peridotite liquidus[21,22] and determine temperature as a function of depth by calculating magma ocean adiabats[20].

We assume that the material that accreted to form Earth and Mars contained the major elements Si, Al, Mg, Fe and Ca in chondritic (C1) proportions before metal–silicate separation[23]. The oxygen contents of chondritic meteorites are variable and poorly defined[24] but, with the exception of enstatite chondrites, the silicate component is generally considerably more oxidized than the Earth's mantle. We therefore vary the amount of oxygen in the starting composition such that between 50 and 80 wt% of the total Fe is present initially as reduced metal, with the remainder being present as an FeO component. These two limits correspond to the non-metallic (silicate) fraction of the chondritic material containing 22 and 10 wt% FeO respectively (for comparison, the Earth's mantle contains ~8 wt% FeO).

The FeO content of the residual silicate mantle, after the metal has segregated, is calculated as a function of magma ocean depth for

Table 1 **Experimental conditions and results**

Run number	Temperature (K)	Pressure (GPa)	log(f_{O_2})	Oxygen (wt%)	ln(K_d)
1,549	2,173	9	−1.82 (0.01)	0.14 (0.01)	−3.218
1,558	2,273	9	−2.08 (0.01)	0.12 (0.01)	−3.077
1,358	2,273	9	−2.67 (0.09)	0.20 (0.09)	−1.903
1,203	2,473	9	−3.59 (0.35)	0.11 (0.35)	−1.525
1,186	2,473	9	−2.06 (0.15)	0.39 (0.15)	−1.945
1,316	2,473	9	−3.55 (0.27)	0.06 (0.27)	−2.189
1,210	2,473	9	−1.47 (0.29)	0.91 (0.29)	−1.776
1,218	2,473	9	−2.84 (0.19)	0.23 (0.19)	−1.574
1,383	2,473	9	−1.47 (0.25)	1.11 (0.25)	−1.585
1,194	2,473	9	−1.24 (0.25	1.28 (0.25)	−1.704
1,371	2,473	9	−1.39 (0.26)	1.12 (0.26)	−1.7
1,352	2,473	9	−1.50 (0.26)	1.06 (0.26)	−1.62
1,547	2,573	9	−2.25 (0.05)	0.38 (0.05)	−1.721
1,312	2,673	9	−1.89 (0.20)	0.78 (0.20)	−1.435
1,551	2,673	9	−1.79 (0.16)	0.79 (0.16)	−1.549
1,273	2,473	18	−2.32 (0.20)	0.14 (0.20)	−2.621
1,275	2,473	18	−2.08 (0.18)	0.27 (0.18)	−2.314
1,285	2,473	18	−1.12 (0.25)	0.62 (0.25)	−2.545

A full list of sample analyses is provided in the Supplementary Information. log(f_{O_2}) is calculated relative to the iron-wüstite buffer; K_d is defined in equation (1).

Earth and Mars (Fig. 3). In the case of Earth, the temperatures of magma oceans with depths <800 km are too low for significant amounts of oxygen to dissolve in the metal phase. Consequently, the initial FeO content of the silicate fraction of the chondritic material is changed only slightly by metal segregation (Fig. 3a). As the magma ocean depth is increased beyond 800 km, however, the amount of oxygen that partitions into the metal increases (owing to higher temperatures) with the consequence that the FeO content of the residual silicate mantle becomes increasingly reduced. Using the simple extrapolation model of equation (2), a magma ocean with a depth of ~1,800 km gives the current FeO content (8 wt%) and Fe/(Fe + Mg) ratio (0.1) of the Earth's mantle, assuming that the starting chondritic material was relatively oxidized with an initial FeO content of the order of 18–22 wt% (Fig. 3a). Considering the model uncertainties, the magma ocean depth could be as low as 1,200 km. A magma ocean with a depth of ≥1,200 km has also been proposed on the basis of siderophile element partitioning studies[2,25–27].

In the case of Mars, the model predicts little change in the FeO content of the residual mantle as a result of core formation, irrespective of magma ocean depth (Fig. 3b). This is because the pressures and temperatures of a martian magma ocean are much lower than on Earth[4]; consequently, little or no oxygen dissolves in the liquid metal because of the low temperatures. Our results therefore show that Earth and Mars could have accreted from material with the same initial FeO content (~18 wt%) and that the different FeO contents of their mantles are a consequence of the partitioning behaviour of oxygen during core formation. The model also explains the different mass fractions of the cores of Earth and Mars because more metal segregates from the magma ocean on Earth (~28 wt%) than on Mars (~18 wt%).

Although the model requires large extrapolations of the experimental data, the associated uncertainties do not affect our conclusions for Earth and Mars (see Supplementary Information). Using existing thermodynamic data[28,29] on pure Fe liquid, oxygen and iron oxide we can calculate a value for ΔS that is in good agreement with our determined value. This calculation indicates that the inclusion of heat capacity functions to determine the temperature dependence of ΔS even up to 6,000 K has a very minor effect on the results of the model. The extrapolation assumes a constant positive value for ΔV of the metal–oxide equilibrium, which means that oxygen solubility decreases with pressure. This trend could reverse, however, at pressures higher than those of our experiments if the value for ΔV becomes negative as a result of compressibility or phase transformation[30]. The martian mantle, however, extends only to pressures of 25 GPa and is therefore within

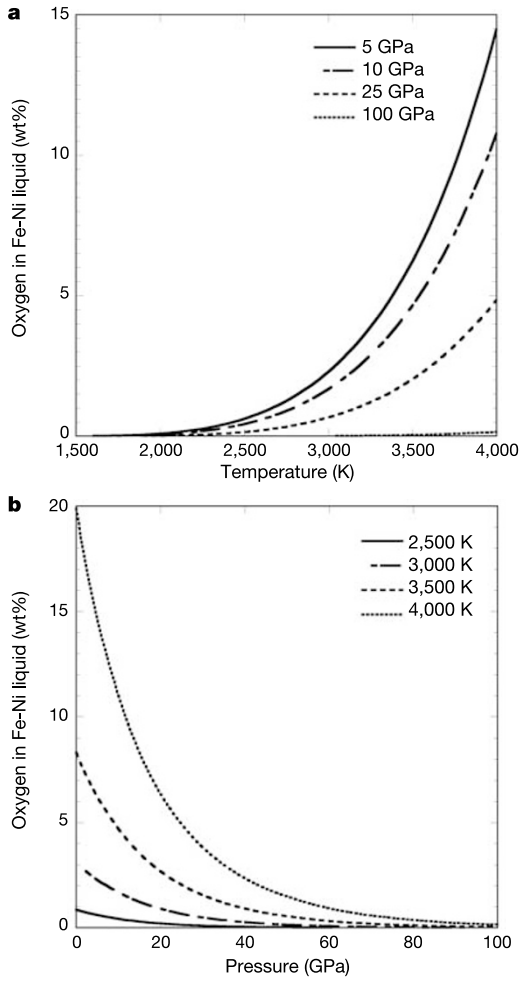

Figure 2 Extrapolations of the oxygen solubility data to higher temperatures and pressures (**a** and **b**) using equation (2). The oxygen fugacity is fixed at two log units below the iron-wüstite buffer.

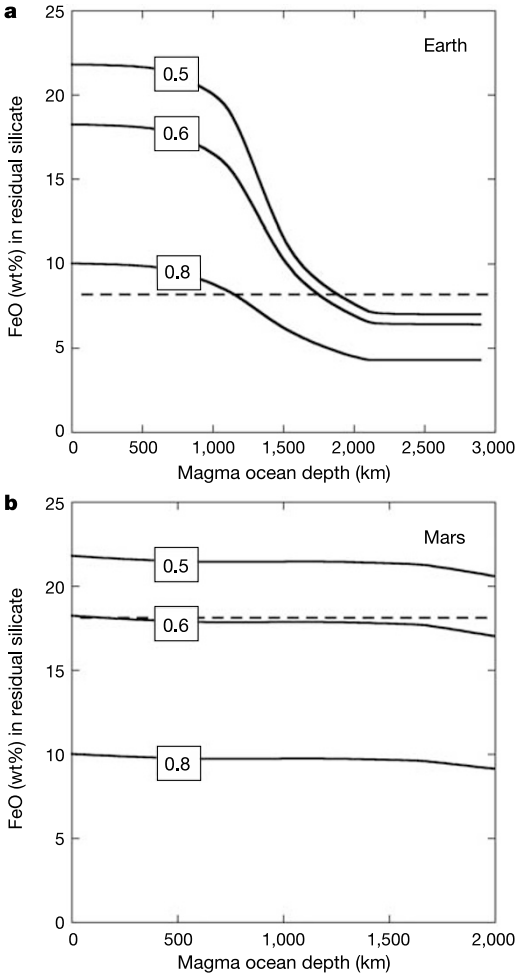

Figure 3 Results of the metal–silicate separation model for Earth (**a**) and Mars (**b**). The FeO contents of the residual silicate mantles (after metal segregation) are shown as a function of magma ocean depth. In each case, the three curves correspond to different initial oxygen contents and are labelled with the weight fraction of Fe that is initially present as metal; the three values correspond to 22, 18 and 10 wt% FeO in the silicate fraction, respectively. The results show that metal–silicate separation in a deep magma ocean would strongly reduce the FeO content of the silicate mantle on Earth, whereas on Mars metal–silicate separation has little effect. The horizontal broken lines indicate the FeO contents of the mantles of Earth and Mars.

the experimental pressure range. If oxygen solubility does increase at pressures higher than 25 GPa, this would reduce the magma ocean depth required on the Earth to satisfy the FeO content of the present-day mantle and make it more likely that oxygen remained dissolved in the metal as it formed the core.

An important consequence for the Earth is that the metal that segregated at the base of the magma ocean would have contained a significant amount of oxygen (for example, 7–8 wt%). As a result of increasing pressure, the solubility of oxygen in Fe-alloy is predicted to decrease with depth below the magma ocean (Fig. 2). There are three possibilities for the fate of the dissolved oxygen, all of which could be important. (1) FeO precipitated from liquid metal between the base of the magma ocean and the proto-core, thus creating chemical heterogeneities that may still exist in the lowermost mantle[8]. (2) Oxygen was transported by liquid metal to the core, where FeO precipitated to form the D″ layer at the core–mantle boundary[9]. (3) At least part of the oxygen may still be dissolved in the core (up to 8 wt% according to our model), thus contributing significantly to its light-element budget[10,11]. If oxygen does become more soluble in liquid metal at pressures higher than our experimental conditions, then that would tend to favour this final possibility. In contrast, the martian core is unlikely to contain any dissolved oxygen, which is consistent with its probable high sulphur content[7]. □

Received 6 October 2003; accepted 8 March 2004; doi:10.1038/nature02473.

1. Li, J. & Agee, C. B. Geochemistry of mantle–core differentiation at high pressure. *Nature* **381,** 686–689 (1996).
2. Li, J. & Agee, C. B. The effect of pressure, temperature, oxygen fugacity and composition on partitioning of nickel and cobalt between liquid Fe-Ni-S alloy and liquid silicate: Implications for the Earth's core formation. *Geochim. Cosmochim. Acta* **65,** 1821–1832 (2001).
3. Righter, K., Drake, M. J. & Yaxley, G. Prediction of siderophile element/silicate partition coefficients to 20 GPa and 2800 °C: the effects of pressure, temperature, oxygen fugacity, and silicate and metallic melt compositions. *Phys. Earth Planet. Inter.* **100,** 115–134 (1997).
4. Righter, K., Hervig, R. L. & Kring, D. A. Accretion and core formation on Mars: molybdenum contents of melt inclusion glasses in three SNC meteorites. *Geochim. Cosmochim. Acta* **62,** 2167–2177 (1998).
5. Anderson, D. L. *Theory of the Earth* (Blackwell, Boston, 1989).
6. Dreibus, G. & Wanke, H. Mars, a volatile-rich planet. *Meteoritics* **20,** 367–381 (1985).
7. McSween, H. Y. Jr What we have learnt about Mars from SNC meteorites. *Meteoritics* **29,** 757–779 (1994).
8. Kellogg, L. H., Hager, B. H. & van der Hilst, R. D. Compositional stratification in the deep mantle. *Science* **283,** 1881–1884 (1999).
9. Garnero, E. J., Revenaugh, J., Williams, Q., Lay, T. & Kellogg, L. H. in *The Core-Mantle Boundary Region* (eds Gurnis, M., Wysession, M. E., Knittle, E. & Buffett, B. A.) 319–334 (Geodynamics Series 28, Am. Geophys. Union, Washington, 1998).
10. Poirier, J.-P. Light elements in the Earth's outer core: A critical review. *Phys. Earth Planet. Inter.* **85,** 319–337 (1994).
11. Hillgren, V., Gessmann, C. K. & Li, J. in *Origin of the Earth and Moon* (eds Canup, R. & Righter, K.) 245–263 (Univ. Arizona Press, Tucson, 2000).
12. Melosh, H. J. in *Origin of the Earth* (eds Newsom, H. E. & Jones, J. H.) 69–83 (Oxford Univ. Press, Oxford, 1990).
13. Stevenson, D. J. in *Origin of the Earth* (eds Newsom, H. E. & Jones, J. H.) 231–249 (Oxford Univ. Press, Oxford, 1990).
14. Gessmann, C. K. & Rubie, D. C. The effect of temperature on the partitioning of Ni, Co, Mn, Cr and V at 9 GPa and constraints on formation of the Earth's core. *Geochim. Cosmochim. Acta* **62,** 867–882 (1998).
15. O'Neill, H. S. C., Canil, D. & Rubie, D. C. Metal-oxide equilibria to 2500 °C and 25 GPa: implications for core formation and the light component in the Earth's core. *J. Geophys. Res.* **103,** 12239–12260 (1998).
16. Kato, T. & Ringwood, A. E. Melting relationships in the system Fe-FeO at high pressures: implications for the composition and formation of the Earth's core. *Phys. Chem. Miner.* **16,** 524–538 (1989).
17. Trønnes, R. G. Melting relations and major element partitioning in an oxidized bulk Earth model composition at 15–26 GPa. *Lithos* **53,** 233–245 (2000).
18. Trønnes, R. G. & Frost, D. J. Peridotite melting and mineral-melt partitioning of major and minor elements at 22–24.5 GPa. *Earth Planet. Sci. Lett.* **197,** 117–131 (2002).
19. Li, J. & Agee, C. B. Element partitioning constraints on the light element composition of the Earth's core. *Geophys. Res. Lett.* **28,** 81–84 (2001).
20. Rubie, D. C., Melosh, H. J., Reid, J. E., Liebske, C. & Righter, K. Mechanisms of metal-silicate equilibration in the terrestrial magma ocean. *Earth Planet. Sci. Lett.* **205,** 239–255 (2003).
21. Herzberg, C. & Zhang, J. Melting experiments on anhydrous peridotite KLB-1: Compositions of magmas in the upper mantle and transition zone. *J. Geophys. Res.* **101,** 8271–8295 (1996).
22. Ohtani, E. Melting temperature distribution and fractionation in the lower mantle. *Phys. Earth Planet. Inter.* **33,** 12–25 (1983).
23. McDonough, W. F. & Sun, S.-s. The composition of the Earth. *Chem. Geol.* **120,** 223–253 (1995).
24. O'Neill, H. S. C. & Palme, H. in *The Earth's Mantle* (ed. Jackson, I.) 3–126 (Cambridge Univ. Press, Cambridge, 1998).
25. Chabot, N. L. & Agee, C. B. Core formation in the Earth and Moon: new experimental constraints from V, Cr and Mn. *Geochim. Cosmochim. Acta* **67,** 2077–2091 (2003).
26. Gessmann, C. K. & Rubie, D. C. The origin of the depletions of V, Cr, and Mn in the mantles of the Earth and Moon. *Earth Planet. Sci. Inter.* **184,** 95–107 (2000).
27. Bouhifd, M. A. & Jephcoat, A. P. The effect of pressure on partitioning of Ni and Co between silicate and iron-rich metal liquids: a diamond-anvil cell study. *Earth Planet. Sci. Inter.* **209,** 245–255 (2003).
28. Chase, M. W. J. *et al.* JANAF thermochemical tables. *J. Phys. Chem. Ref. Data* **14** (suppl. 1) (1985).
29. Sundman, B. An assessment of the Fe-O system. *J. Phase Equil.* **12,** 127–140 (1991).
30. Fei, Y. & Mao, H.-K. In situ determination of the NiAs phase of FeO at high pressure and temperature. *Science* **266,** 1678–1680 (1994).

Supplementary Information accompanies the paper on **www.nature.com/nature**.

Acknowledgements We thank H. Fischer, G. Herrmannsdörfer, D. Krausse and H. Schulze for technical assistance. The German Science Foundation (DFG) supported this research.

Competing interests statement The authors declare that they have no competing financial interests.

Correspondence and requests for materials should be addressed to D.C.R. (dave.rubie@uni-bayreuth.de).

Convergent evolution in mechanical design of lamnid sharks and tunas

Jeanine M. Donley[1], Chugey A. Sepulveda[1], Peter Konstantinidis[2], Sven Gemballa[2] & Robert E. Shadwick[1]

[1]*Marine Biology Research Division, Scripps Institution of Oceanography, University of California San Diego, La Jolla, California 92093-0202, USA*
[2]*Department of Zoology, University of Tübingen, Auf der Morgenstelle 28, D-72076 Tübingen, Germany*

The evolution of 'thunniform' body shapes in several different groups of vertebrates, including whales, ichthyosaurs[1] and several species of large pelagic fishes[2] supports the view that physical and hydromechanical demands provided important selection pressures to optimize body design for locomotion during vertebrate evolution. Recognition of morphological similarities between lamnid sharks (the most well known being the great white and the mako) and tunas has led to a general expectation that they also have converged in their functional design; however, no quantitative data exist on the mechanical performance of the locomotor system in lamnid sharks. Here we examine the swimming kinematics, *in vivo* muscle dynamics and functional morphology of the force-transmission system in a lamnid shark, and show that the evolutionary convergence in body shape and mechanical design between the distantly related lamnids and tunas is much more than skin deep; it extends to the depths of the myotendinous architecture and the mechanical basis for propulsive movements. We demonstrate that not only have lamnids and tunas converged to a much greater extent than previously known, but they have also developed morphological and functional adaptations in their locomotor systems that are unlike virtually all other fishes.

During their 400 million years of independent evolution, sharks and bony fishes have diverged in many fundamental aspects of their anatomy and physiology. However, two groups of dominant open-ocean predators, the lamnid sharks and the tunas, even when looked at superficially, display remarkably similar morphological specializations related to locomotion[3–12] (Fig. 1a). The shared characteristics in these distantly related groups that distinguish them from virtually all other fish have arisen independently, probably as the result of selection for fast and continuous locomotion. Moreover, in both lamnids and tunas, the aerobic (red) musculature that powers cruise swimming is concentrated in a more medial (closer to the